Examination of evidence for resonances at high excitation energy in the 7α disassembly of ^{28}Si

X. G. Cao, E. J. Kim, K. Schmidt, K. Hagel, M. Barbui, J. Gauthier, S. Wuenschel, G. Giuliani, M. R. D. Rodriguez, S. Kowalski, H. Zheng, M. Huang, A. Bonasera, R. Wada, N. Blando, G. Q. Zhang, C. Y. Wong, A. Staszczak, Z. X. Ren, Y. K. Wang, S. Q. Zhang, J. Meng, and J. B. Natowitz

Phys. Rev. C **99**, 014606 — Published 7 January 2019

DOI: 10.1103/PhysRevC.99.014606

Evidence for resonances at high excitation energy in the 7α disassembly of ^{28}Si

X. G. Cao,[1,2,3,4] E. J. Kim,[2,5] K. Schmidt,[6,2] K. Hagel,[2] M. Barbui,[2] J. Gauthier,[2] S. Wuenschel,[2] G. Giuliani,[2,7] M. R. D. Rodriguez,[2,8] S. Kowalski,[6] H. Zheng,[2,9] M. Huang,[2,10] A. Bonasera,[2,7] R. Wada,[2] N. Blando,[2] G. Q. Zhang,[1,2] C. Y. Wong,[11] A. Staszczak,[12] Z. X. Ren,[13] Y. K. Wang,[13] S. Q. Zhang,[13] J. Meng,[13,14] and J. B. Natowitz[2]

[1]*Shanghai Institute of Applied Physics, Chinese Academy of Sciences, Shanghai 201800, China*
[2]*Cyclotron Institute, Texas A&M University, College Station, Texas 77843*
[3]*Shanghai Advanced Research Institute, Chinese Academy of Sciences, Shanghai 201210, China*
[4]*Zhangjiang Laboratory, Shanghai 201210, China*
[5]*Division of Science Education, Chonbuk National University, 567 Baekje-daero Deokjin-gu,Jeonju 54896, Korea*
[6]*Institute of Physics, University of Silesia, 40-007 Katowice, Poland.*
[7]*Laboratori Nazionali del Sud, INFN, via Santa Sofia, 62, 95123 Catania, Italy*
[8]*Instituto de Física, Universidade de São Paulo, Caixa Postal 66318, CEP 05389-970, São Paulo, SP, Brazil*
[9]*School of Physics and Information Technology, Shaanxi Normal University, Xi'an 710119, China*
[10]*College of Physics and Electronics Information, Inner Mongolia University for Nationalities, Tongliao, 028000, China*
[11]*Physics Division, Oak Ridge National Laboratory, Oak Ridge, USA*
[12]*Institute of Physics, Maria Curie-Skłodowska University, Lublin, Poland*
[13]*State Key Laboratory of Nuclear Physics and Technology, School of Physics, Peking University, Beijing 100871, China*
[14]*Yukawa Institute for Theoretical Physics, Kyoto University, Kyoto 606-8502, Japan*

(Dated: December 7, 2018)

The experimental excitation function for the 7α de-excitation of ^{28}Si nuclei excited to high excitation energies in the collisions of 35 MeV/nucleon ^{28}Si with ^{12}C reveals resonance structures. The possibility that these structures may indicate the population of toroidal high-spin isomers such as those predicted by a number of recent theoretical calculations is discussed and the need for further investigations is emphasized.

PACS numbers: 25.70.Pq
Keywords: Intermediate energy heavy ion reactions, Clusters

I. INTRODUCTION

Light nuclei in their ground states in the valley of stability usually have spherical or near-spherical geometries [1]. With increasing excitation energy and/or angular momentum, these nuclei may exhibit more exotic shapes [2–5]. Theoretical investigations of the possible existence of extremely exotic nuclear shapes have a long history. Wheeler suggested that, under certain conditions, nuclei could assume toroidal shapes [3]. Pursuing this suggestion, Wong explored possible toroidal and bubble nuclei and predicted exited toroidal states in the mass region of $40 \lesssim A \lesssim 70$ and $A \lesssim 250$ [6–8]. Large shell effects in light nuclei and large Coulomb energies in heavy nuclei favor exotic toroidal configurations. A recent search for heavy toroidal systems indicated that the probability of planar fragmentation configurations in the experimental data was much greater than predicted by quantum molecular dynamics calculations [9].

Extending such studies Wong and collaborator predicted that, toroidal configurations were also possible for nuclei with a sufficiently high angular momenta [10–12]. They defined the region of mass and angular momentum in which such configurations might be realized. More recent theoretical studies have used microscopic techniques to address this question of light toroidal nuclei. In particular, Zhang *et al*. [13], Ichikawa *et al*. [14, 15] and Staszczak and Wong [16–18], using varied approaches, have predicted the existence of toroidal isomers in light nuclei.

We can understand the origin of possible light-A toroidal isomers in the following simple way. In a nucleus with a toroidal shape, there are toroidal magic numbers $2(2m + 1)$, with integer $m \geq 1$, arising from large energy gaps between single-particle levels in the light mass region (Fig. 1 of [6]). Extra stability [19] associated with toroidal magic numbers leads to an excited local energy minimum that is stable against the expansion and contraction of the toroidal major radius (see Fig. 2 of [6], Fig. 18 of [7], and Fig. 1 of [13]). Such an excited state residing in a local energy minimum under a toroidal shape constraint will be called a diabatic state, and the corresponding constrained calculation a diabatic calculation [13]. This is in contrast to an adiabatic state of the lowest energy minimum in an adiabatic calculation without a shape constraint [14–18]. Relative to a diabatic toroidal local energy minimum core, Bohr-

TABLE I: Calculated parameters for the predicted toroidal isomer in ^{28}Si. Left to right: Spin I=I_z, quadrupole moment Q_{20}, the cranking rotation frequency $\hbar\omega$, excitation energy E_x, toroidal major radius R, minor radius d, aspect ratio R/d, and maximum density $\rho_{\max}$

	I [$\hbar$]	Q_{20} [b]	$\hbar\omega$ [MeV]	E_x [MeV]	R [fm]	d [fm]	R/d	$\rho_{\max}$ [fm^{-3}]
^{28}Si	44	-5.86	2.8	143.18	4.33	1.45	2.99	0.119

Mottelson spin-aligning particle-hole excitations [20] can be constructed to yield a yrast toroidal nucleus with a spin, I=I_z, by promoting nucleons with angular momentum aligned opposite to a chosen symmetry axis to populate orbitals with angular momentum aligned along the symmetry axis [14–18]. The spinning toroidal nucleus possesses an effective "rotational" energy that tends to expand the toroid, whereas the energy associated with the nuclear bulk properties tends to contract the toroid. The balance between the two energies gives rise to a local toroidal energy minimum [8]. For small values of I, the toroidal minimum occurs as an excited (diabatic) state above the sphere-like ground states. As I increases, the crossing of the toroidal and sphere-like energy surfaces takes place, and the toroidal high-spin energy minimum switches to become the lowest energy (adiabatic) state. Adiabatic self-consistent calculations have located an extensive region of toroidal high-spin isomer (THSI) states that are stable against the expansion and contraction of the toroids [14–18].

Motivated by the predictions of toroidal isomeric states in a number of light nuclei, we have undertaken searches for evidence of their existence. For ^{28}Si, the nucleus investigated in the present work, the Staszczak and Wong calculations indicate that toroidal shapes with I= 0 become possible at excitation energies greater than 85 MeV. The existence of a stabilized state with angular momentum of 44$\hbar$ and excitation energy of 143.18 MeV [16] was predicted. See Table 1.

In the calculation the toroidal shape of this short-lived isomer ^{28}Si is characterized by a radius of 4.33 fm and a cross sectional radius of 1.45 fm for the cylindrical ring containing the nucleons. Thus the aspect ratio is 2.99. The predicted toroidal states, although expected at very high energies, are analogous to yrast traps already observed in more conventionally shaped nuclei [21]. Should such very highly excited stabilized toroidal states of light nuclei exist, their lifetimes should be short. They may de-excite or undergo shape relaxation rather quickly. In either case the most-likely de-excitation modes are particle or cluster emission and fragmentation [22].

It is well documented that macroscopic toroids fragment as a result of the development of Plateau-Rayleigh instabilities [23–27]. In the basic Rayleigh description [24] the dominance of a single mode of symmetric fragmentation leads to disassembly into equal size pieces, the number of which is of the order of the aspect ratio of the toroid [23–27]. This correspondence is most accurate for large aspect ratios [26]. Modern numerical simulations taking into account the viscosity of the fluid and the surrounding medium indicate that more complicated symmetric breakups involving different size fragments are possible [27].

As has been already discussed in the literature, nuclear tori might also manifest Plateau-Rayleigh instabilities [6, 7, 11]. The aspect ratio predicted by Staszczak and Wong for the 143.18 MeV, 44$\hbar$ state in ^{28}Si suggests that, while other fragmentations are possible [26], the dominant instability of that toroid would lead to a break-up into $\sim$ 3 fragments. However the actual dominant mode will be affected by the temperature dependent viscosity of the disassembling nucleus [28]. In the nuclear case the discreteness of the nucleons, the existence of Coulomb forces, shell effects and variations in the fragment binding energies may also modify the fragmentation pattern of the torus.

While strongly reduced Coulomb energies might be expected to provide a signature for the disassembly of predicted heavy or super-heavy nuclear toroids in their meta-stable ground-states [8, 9], this is probably not so for the predicted high spin light tori. These light tori are predicted to have very high excitation energies. Thus, in their disassembly, a lowering of the Coulomb repulsion between fragments is probably not observable as the release of large deformation and rotational energies will normally lead to large kinetic energies for the observed decay fragments. Finally, given the high excitation energies involved, it is likely that the initial fragments will often be excited and undergo subsequent de-excitations, smearing the signature of a Plateau-Rayleigh instability.

All of these considerations suggest that judicious choices of reaction mechanism, exit channels and observables will be necessary to probe the possible existence of these very exotic and very interesting nuclei.

Two notable features of the Staszczak-Wong and Ichikawa calculations are that

1. the cross-sectional radii of the cylindrical rings containing the nucleons are $\sim$ 1.5 fm, essentially equal to the α-particle radius. Indeed, in their search for isomeric states in ^{40}Ca, Ichikawa *et al.* used a ring of 10 α-particles as an initial configuration for their cranked Hartree Fock calculations [14].

2. the toroidal rings corresponding to the predicted isomers have matter densities approximately 2/3 of ρ_0 where ρ_0 is the normal central density of such nuclei [15–17] .

Since the general importance of α-like correlations in the structure and properties of light nuclear systems at normal and reduced densities is now well established [29–34], the features noted here suggest that the disassembly

into α-particles or α-conjugate nuclei might be favored for light nuclear toroids. In 1986 Wilkinson specifically suggested that spinning rings of α-particles might be stabilized by circumnavigating neutrons. He discussed their stabilities toward electromagnetic or fragmenting de-excitations and the possibility of producing them in heavy ion collisions [35]. The idea of stabilization by surrounding neutrons is also a feature of the extended Ikeda diagram systematics [36].

We have searched for possible evidence of toroidal isomers in the disassembly of ^{28}Si produced in near-fermi-energy collisions of ^{28}Si with ^{12}C. While some nucleon transfer and nucleon-nucleon collisions leading to early (pre-equilibrium)particle emission occur [37–43], such collisions, many of which lead to essentially binary exit channels, are capable of producing projectile like nuclei in the A=28 mass region with high excitation energy and high angular momentum. Calculations [39–43]indicate that an angular momentum in the range of $40\hbar$ and an excitation energy as high as 170 MeV can be reached. These calculations should be considered as only indicative of possible angular momentum range as they do not have the ingredients to explore detailed quantum structure at such high excitation and angular momentum. When the excitation energy E and the angular momentum I of an emerging ^{28}Si* corresponds to that of a toroidal high-spin isomer, the collective cranking motion and the rearrangement of the single-particle motion of the nucleons may eventually lead to the toroidal high-spin isomer.

Here we report results for an investigation of ^{28}Si, focusing on the 7α decay channels of excited projectile-like fragments produced in the reaction 35 MeV/nucleon ^{28}Si + ^{12}C. In this reaction the energy available in the center of mass is 294 MeV. Interpolation of the systematic calculations of reference [44] indicate that the maximum angular momentum, L_{max}, is $94\hbar$ (a reaction cross section of 2417 mb), L_{crit} for fusion is $26\hbar$ and the rotating liquid drop limiting angular momentum is $40\hbar$. These parameters indicate that the bulk of the reaction cross section will lead, not to fusion, but to initially binary configurations of excited projectile-like and target-like nuclei. This is consistent with experimental results reported for similar collisions in this energy region [37, 38].

EXPERIMENTAL DETAILS

The experiment was performed at Texas A&M University Cyclotron Institute. A 35 MeV/nucleon ^{28}Si beam produced by the $K500$ superconducting cyclotron impinged on a ^{12}C target. The reaction products were measured using a 4π array, NIMROD-ISiS (Neutron Ion Multidetector for Reaction Oriented Dynamics with the Indiana Silicon Sphere) [45, 46] which consisted of 14 concentric rings covering from 3.6° to 167° in the laboratory frame [45]. In the forward rings with $\theta_{lab} \leq 45°$, two special modules were set having two Si detectors (150 and 500 μm) in front of a CsI(Tl) detector ($3-10$ cm), referred to as super-telescopes. The other modules (called telescopes) in the forward and backward rings had one Si detector (one of 150, 300 or 500 μm) followed by a CsI(Tl) detector. The pulse shape discrimination method was employed to identify the light charged particles with $Z \leq 3$ in the CsI(Tl) detectors. Intermediate mass fragments (IMFs), were identified with the telescopes and super-telescopes using the "$\Delta E - E$" method. In the forward rings an isotopic resolution up to $Z = 12$ and an elemental identification up to $Z = 20$ were achieved. In the backward rings only $Z = 1 - 2$ particles were identified, because of the detector energy thresholds. In addition, the Neutron Ball surrounding the NIMROD-ISiS charged particle array provided information on average neutron multiplicities for different selected event classes. Further details on the detection system, energy calibrations, and neutron ball efficiency can be found in [37, 46, 47].

It is important to note that for these light systems in this energy range the increasing thresholds with increasing laboratory angle lead to a condition in which the efficiencies strongly favor detection of projectile like fragments from mid- peripheral events. Modeling of these collisions using an Antisymmetrized Molecular Dynamics (AMD) code [39] and applying the experimental filter demonstrates that binary type events dominate and that filtering though the detector geometric acceptance and applying the relevant energy thresholds suppresses the slower target-like fragment (TLF) source.

The smallest energy of detected α-particle in 7α events is about 3.3 MeV in the lab frame. Thresholds are similar for other α-conjugate exit channels. Using the AMD+GEMINI simulation analysis before and after experimental filtering, we estimate the detection efficiency for 7α events to be 0.108. The detected event numbers of 6α, 7α and 8α events are 24849, 6467, and 840, respectively. The ratio between them is 1:0.26:0.03.

Nucleons are emitted during the initial phase of the collision. They are often modeled as emission from a *virtual* mid-rapidity source having a velocity close to that of the nucleon-nucleon collision frame [40]. While these nucleons, ejected prior to equilibration of the remaining system, are not from the de-excitation of the primary exit channel products, some of them appear in the projectile velocity region. They should not be included in the calorimetric determination of the *thermalized* excitation energy.

ANALYSIS

For the ^{28}Si+^{12}C reaction, a total of 17.5 million events were recorded and a significant proportion of events had significant α-like (AL) mass emission(i.e. α-particles or α-conjugate nuclei). About 3.19×10^5 events had AL=28.

Of these 6467 detected events had 7 α-particles.

The AMD calculations indicate that for detected A=28 channels $\sim 90\%$ of the nucleons originate from the projectile. Some mixing is consistent with damped collisions. A very careful inspection of experimental invariant velocity plots for each reaction channel and each emitted species confirmed that projectile like sources were strongly dominant in the detected events, except for Z=1 particles. These Z=1 particles showed some contribution from both target-like and mid-rapidity sources, the latter characteristic of pre-equilibrium emission. The observed source velocities for the selected A=28 events decrease slowly with exit channel complexity but are always above the center of mass velocity. Complete fusion is a rare process and target like fragments are generally not detected as indicated above. Searching for 8α events we found that their yield was a factor of 10 less than for 7α events. This indicates small possibility of contamination from such events. All of these features were taken into account in the following analysis.

To characterize the source excitation energies involved we have used calorimetric techniques to determine the excitation energy, E_x, of the primary projectile-like fragments. E_x, is normally defined as the sum of the kinetic energies of ejected particles and fragments in the frame of the total projectile-like nucleus (determined by reconstruction of the mass and velocity of the primary excited nucleus from its de-excitation products) minus the reaction Q-value. This can be generalized as:

$$E_x = \Sigma_{i=1}^{M_{cp}} K_{cp}(i) + M_n < K_n > -Q \qquad (1)$$

where M_{cp} is the multiplicity of charged particles, K_{cp} is the kinetic energy of a charged particle in the source frame, M_n is the neutron multiplicity and $< K_n >$ is the average neutron kinetic energy in the source frame. For the α-conjugate de-excitation channels of ^{28}Si M_n is 0.

The events initially selected typically had a few Z=1 particles (and neutrons) and, in very rare cases, a heavier fragment, associated with them. In our event selection, which focusses on the α-conjugate exit channels, we have allowed Z=1 particles and neutrons in the events but we have determined the excitation energies excluding the energies of Z= 1 particles and neutrons as they are primarily pre-equilibrium particles, representing energy dissipation but not energy deposition into the projectile-like fragment [40]. Invariant velocity plots for the α-particles indicated that the α-particles resulting from mid-rapidity pre-equilibrium emission were negligible and that the small number detected from the target like source (given the thresholds and geometry of the NIMROD detector) could be effectively removed by rejection of α-particles with energies greater than 40 MeV in the projectile-like fragment source frame.

In Figure 1 we present the excitation functions derived in this manner for the α-conjugate exit channels. For comparison, results from calculations using the phenomenological event generator HIPSE [43] and the AMD transport model with a GEMINI afterburner are also presented [39, 41]. While the agreement between the data, the AMD and the HIPSE results is generally good, we note that the 7α, 2 ^{12}C + α and ^{16}O+^{12}C exit channel results differ somewhat from the results of the model calculations. In particular , above 100 MeV excitation energy, the experimental 7α spectrum appears to have statistically significant structure. In the following we focus on this exit channel.

Two hybrid codes, AMD-GEMINI [39, 41, 42] and HIPSE-GEMINI [41–43] were also used to calculate the 7α excitation energy spectrum. The modeling of light particle emission using the code GEMINI was thoroughly examined in reference [42]. In that work, formulations of the barriers and transmission coefficients, the level density and the yrast line were carefully explored. We have used the default parameter prescriptions derived from this work. Results of both calculations, filtered through the NIMROD acceptance and normalized to the data, are also presented in the figure. It is not expected that high energy resonances could appear in these models and, indeed, both are structure-less. The AMD results are somewhat broader in energy and shifted to slightly higher energy than the HIPSE results.

As will be seen in this figure, the 7α distribution spans the energy region in which toroidal configurations are predicted and the 143.18 MeV stabilized state is predicted to exist. After reaching a maximum at $\sim$ 110 MeV the excitation energy distribution shows some structure at 126 and 138 MeV. The granularity and angular resolution of NIMROD-ISiS are not ideally suited to searches such as this, as the transformation to the source frame relies upon the angle of detection. Through simulations we have determined that the observed experimental width in excitation energy of an initially sharp state at 140 MeV will have a standard deviation, σ, of $\sim$ 4 MeV resulting from the angular uncertainty. Taking this into account, the broad structures apparent in the excitation energy spectrum are consistent with much narrower resonances in the excitation energy distribution. We have checked this by adding a 7α delta function with Ex=143 MeV to the uncorrelated 7α events and observing that the resultant filtered spectrum is consistent with our observed spectrum. Clearly an experiment with much better angular resolution, allowing better resolution for the excitation energy spectrum, would be very desirable.

In figure 2(a), we compare the experimental spectrum for the 7α events to an uncorrelated 7α spectrum. The spectrum of uncorrelated events was constructed by randomly selecting 7 α-particles from 7 different events. The random selection was done many times to assure that the statistical fluctuations for this spectrum would be much lower than those of the correlated event spectrum. This uncorrelated spectrum is taken to represent the 7α phase

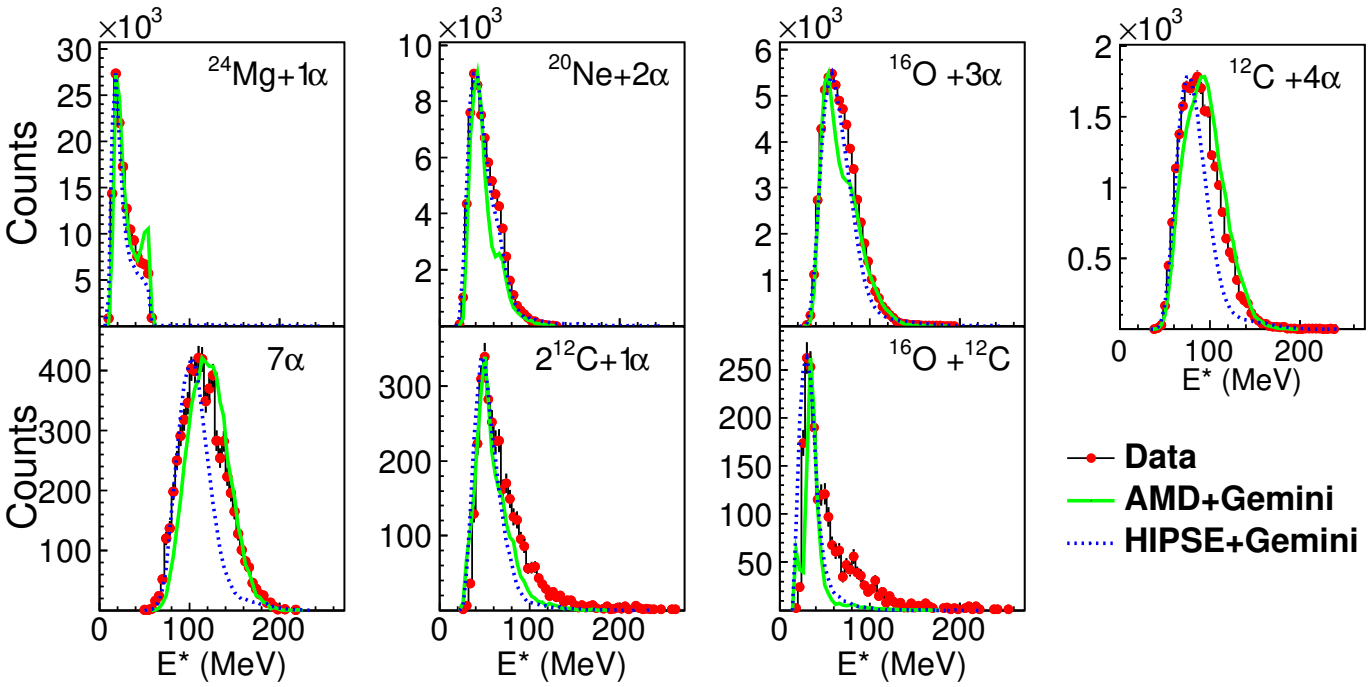

FIG. 1: Excitation functions for the α-conjugate exit channels in the de-excitation of ^{28}Si. The shapes of the experimental data are compared with results of both AMD and HIPSE calculations.

space in this excitation energy region. Subtracting the normalized uncorrelated spectrum from the data results in the difference spectrum depicted in Figure 2(b). Some excess is seen at 114 MeV. The peaks at 126 and 138 MeV are quite prominent and there is a tailing toward higher energies. The under-shoot at 100 MeV and below may suggest that the normalization of the uncorrelated spectrum is too conservative. If that spectrum is lowered the peaks in the difference spectrum will be even more prominent. For comparison we have also employed the AMD calculated spectrum as a background spectrum to be subtracted from the experimental spectrum. For this purpose the AMD-GEMINI spectrum was shifted to agree with the experimental uncorrelated spectrum at the lower edge of the experimental spectrum.

The difference spectrum obtained by subtracting the normalized AMD- GEMINI spectrum from the experimental data, is very similar to, but not exactly the same as that obtained when subtracting the experimental uncorrelated spectrum from the experimental data.

The structure in the experimental 7α spectrum appears to reflect mechanisms not encompassed in the dynamic reaction models or normal statistical decay treatments. Relative to the uncorrelated background derived from the experiment the statistical significance of the difference peak at 114 MeV is 5.0σ, at 126 MeV is 7.9σ and at 138 MeV is 7.1σ [48]. We take these to be the minimum values for the statistical significance since the construction of the uncorrelated spectrum includes contributions from the peak region and the number of uncorrelated α-particles may, therefore, be overestimated in that region.

Evaluation of the statistical significance of the observed peaks is sensitive to the background assumed. If we base the test for the statistical significance on the use of the AMD GEMINI result we find a statistical significance of 114, 126 and 138 MeV peaks to be 4.2σ, 6.0σ , and 6.6σ, respectively.

CROSS SECTION AND ANGULAR MOMENTUM

To determine the cross section for the 7α channel we have assumed that the total events detected with our minimum bias trigger (1 particle or 1 fragment detected), corrected for detector efficiency, represent a total reaction cross section of 2417 mb [44]. The overall detector efficiency was determined from the ratio of numbers of AMD-GEMINI generated events before and after the detector filter. The specific efficiency for the 7α channel was also determined in a similar fashion. Because double hit corrections can be large, these results are very sensitive to the number of, and excitation energies of intermediate ^{8}Be nuclei produced. Thus there may be a significant systematic uncertainty in the resultant cross section. Based on the estimated uncertainties we estimate the cross section for the 7α channel to be 1.9 mb with a systematic uncertainty of $\sim$ 25%. We estimate

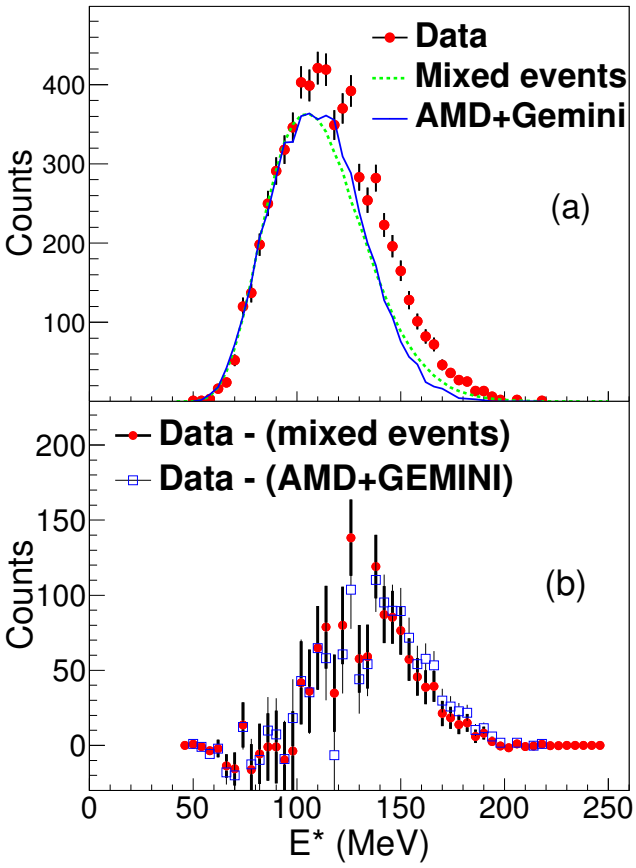

FIG. 2: Excitation energy distribution leading to observed 7α events. Top Panel - the data are represented by solid red circles. An uncorrelated spectrum derived from event mixing is represented by the solid blue line. The filtered result from an AMD-GEMINI calculation is indicated by the dashed and dotted green line (see text). The last two are normalized to the experimental spectrum at the lower edge of the spectrum. On the bottom panel the differences between the experimental spectrum and the others are presented. Relative to the uncorrelated background derived from the experiment the statistical significance of the difference peak at 114 MeV is 5.0σ, at 126 MeV is 7.9σ and at 138 MeV is 7.1σ. See text

the cross sections for the 126 and 138 MeV peaks, respectively, to be 51μb and 28μb with similar uncertain ties.

If the state observed at 138 MeV corresponds to the predicted 143.18 MeV toroidal state the angular momentum would be $44\hbar$. Our results give no direct information on the angular momentum. As already noted, the AMD and HIPSE calculations, employing semi classical techniques, indicate that angular momenta in the range of $40\hbar$ are reached but they do not have the ingredients necessary to explore detailed structure at such high excitation energy and angular momentum.

MOMENTUM SPACE SHAPE ANALYSES

We have utilized a shape analysis technique [49, 50] to diagnose the momentum space source shape for the 7α events. This type of analysis is a popular method to study emission patterns of sources, dynamical aspects of multi-fragmentation and collective flows of particles in heavy ion collisions at intermediate and relativistic energies. Although we are not able to observe directly the geometric shape of these sources, the momentum space correlations among the detected fragments provide hints of shapes and information on the disassembly dynamics. Should nuclei with exotic shapes undergo simultaneous fragmentation into equal sized cold fragments the observed momentum space distributions of products would be directly related to the initial geometric configuration of the de-exciting system. In contrast, if the primary fragments are excited or the emission is sequential, de-excitation of the initially produced fragments could significantly modify the initial momentum space distribution. For the light α-conjugate nuclei explored in this study, α-emission from excited heavier primary fragments would produce large perturbations of that distribution.

The analysis employs a tensor constructed from the product momenta, written as: $T_{ij} = \Sigma_{\nu=1}^{N} p_i^\nu p_j^\nu$ where N is the total number of particles, p_i^ν is the momentum component of ν^{th} particle in the center-of-mass and i refers to the Cartesian coordinate. The tensor can be diagonalized to reduce the event shape to an ellipsoid. The eigenvalues of the tensor: λ_1, λ_2 and λ_3 , normalized by: $\lambda_1 + \lambda_2 + \lambda_3 = 1$ and ordered according to: $\lambda_1 \leq \lambda_2 \leq \lambda_3$, can quantitatively give shape information of the events. The sphericity is defined as: $S = \frac{3}{2}(1 - \lambda_3)$, and coplanarity is defined as: $C = \frac{\sqrt{3}}{2}(\lambda_2 - \lambda_1)$. In the sphericity-coplanarity plane, the ideal rod, disk and sphere events are exactly located at the three vertices of the triangle: (0,0) (3/4, $\sqrt{3}$/4) and (1,0), respectively. Two fragment events will always appear at 0,0 while three fragments events will appear on the rod-disk axis. To appear as a disk at the apex of this triangle requires a simultaneous and symmetric fragmentation into 3 or more equally sized pieces.

The results of the momentum shape analysis are shown in Fig. 3(a). While there are some events located in the disk region, the bulk of the events are elsewhere. Also depicted in Figure 3 are sphericity-coplanarity plots of the AMD-GEMINI results. Figure 3(b) portrays the filtered final results. Figure 3(c) presents the plot for the 300 fm/c freezeout momentum distribution predicted by AMD. Clearly this freeze-out distribution is much more rod to disk like than that observed after de-excitation and filtering. The momentum space shape analysis results suggest that, if toroidal configurations are produced, the observed final distribution normally results

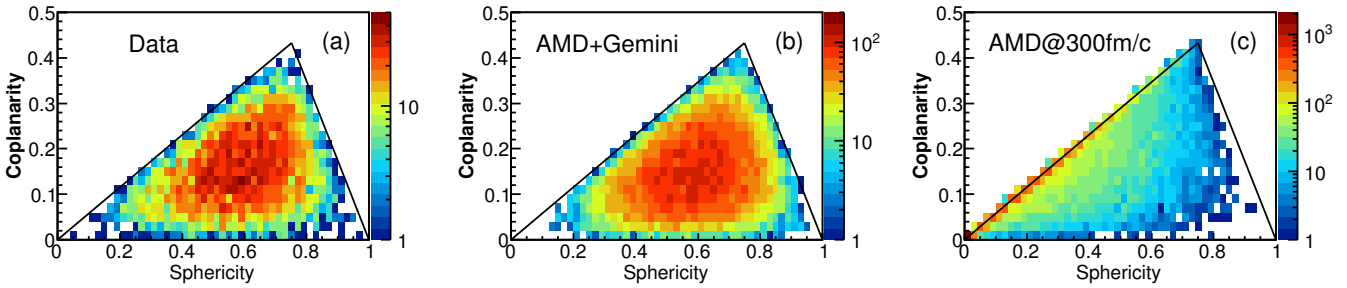

FIG. 3: Shape analysis of 7α events in the de-excitation of AL = 28, Z = 14 projectile-like nuclei produced in the 35 MeV/nucleon ^{28}Si + ^{12}C reaction. Left-Experimental data. Middle-Filtered results from AMD-GEMINI calculation. Right- Results for AMD primary fragments at 300 fm/c.

from processes in which an initial breakup into larger excited fragments is followed by α-particle de-excitation of those fragments.

COMPARISON WITH TOROIDAL SHELL MODEL

The 7α de-excitation of ^{28}Si projectile-like fragments encompasses the excitation energy range for which toroidal configurations are predicted to exist. The resonance structure indicates the existence of stabilized configurations which may correspond to toroidal high-spin states such as those predicted in several theoretical calculations [13–18]. If the observed state at 138 MeV corresponds to the 143.18 MeV state predicted to exist by Staszczak and Wong [16], the angular momentum would be $44\hbar$.

Resonances at such high excitation energies are rather unusual, and we know of no model except the toroidal isomer model that predicts ^{28}Si* resonances at these high excitation energies. Thus, We have attempted to explore whether the experimental data may be described in terms of the toroidal shell model in which nucleons move in the toroidal potential $V(\rho,z) = \frac{1}{2}m\omega_0^2(\rho-R)^2 + \frac{1}{2}m\omega_0^2 z^2$ [6, 7, 16]. Upon neglecting the small spin-orbit interaction, the toroidal single-particle energy $\epsilon(n\Lambda\Omega)$ for the $|n\Lambda\Omega\rangle$ state, in the I=0 toroidal core with a major radius R and $R \gg d$, is approximately

$$\epsilon(n\Lambda\Omega) \approx \hbar\omega_0(n+1) + \frac{\hbar^2\Lambda^2}{2mR^2}, \qquad (2)$$

where n=n_z+n_ρ is the harmonic oscillator quantum number, ω_0 the oscillator frequency, m the nucleon mass, Λ the orbital angular momentum about the symmetry z-axis, Ω_z=Λ+s_z, and s_z the intrinsic nucleon spin.

Relative to the toroidal I=0 core at E_0 occupying the lowest toroidal single-particle states, the spin-aligning Bohr-Mottelson particle-hole excitations leading to toroidal high-spin isomers can be constructed by following the crossings of Routhian energy levels as a function of increasing cranking frequency $\hbar\omega$ (Fig. 1(b) of [16]). The contribution to ΔI_z and $\Delta(E_I - E_0)$ from a particle-hole excitation can be easily obtained from the changes in particle-hole state quantum numbers $(n\Lambda\Omega)$ and $\epsilon(n\Lambda\Omega)$. For ^{28}Si, for example, the 1p-1h excitation contributes ΔI_z=$8\hbar$, and $\Delta(E_I - E_0)$=$7\hbar^2/2mR^2$ by promoting a nucleon from $|03(-7/2)\rangle$ to $|04(9/2)\rangle$. Similar contributions can be obtained for the 2p-2h excitation by additional promotion from $|03(-5/2)\rangle$ to $|04(7/2))\rangle$, 3p-3h from $|02(-5/2)\rangle$ to $|05(11/2)\rangle$, and 4p-4h from $|02(-3/2)\rangle$ to $|05(9/2)\rangle$. From such calculations, we obtain the spin I=I_z and the relative energy $(E_I - E_0)$ (in units of $(\hbar^2/2mR^2)$), for various ^{28}Si* toroidal high-spin isomer states as the signature for toroidal ^{28}Si* in Table II.

TABLE II: Toroidal high-spin isomers (THSI) of ^{28}Si* in the toroidal shell model. The spin-aligning (n particle)-(n hole) excitations, for neutrons (ν) and protons (π), relative to a toroidal core with I=0 and energy E_0, lead to the THSI state of spin I=I_z, and excitation energy E_I.

Configurations	I	$(E_I - E_0)$ in $\hbar^2/2mR^2$	E_I (MeV)
$(0p\text{-}0h)_\nu(0p\text{-}0h)_\pi$	0	0	91.82
$(1p\text{-}1h)_\nu(1p\text{-}1h)_\pi$	16	14	101.2
$(0p\text{-}0h)_\nu(2p\text{-}2h)_\pi$+$(2p\text{-}2h)_\nu(0p\text{-}0h)_\pi$	14	14	101.2
$(2p\text{-}2h)_\nu(2p\text{-}2h)_\pi$	28	28	110.58
$(2p\text{-}2h)_\nu(3p\text{-}3h)_\pi$+$(3p\text{-}3h)_\nu(2p\text{-}2h)_\pi$	36	49	124.65
$(3p\text{-}3h)_\nu(3p\text{-}3h)_\pi$	44	70	138.72
$(3p\text{-}3h)_\nu(4p\text{-}4h)_\pi$+$(4p\text{-}4h)_\nu(3p\text{-}3h)_\pi$	50	91	152.79
$(4p\text{-}4h)_\nu(4p\text{-}4h)_\pi$	56	112	166.86

We can identify the I=$44\hbar$, $36\hbar$ and $28\hbar$ toroidal high-spin isomers in the toroidal shell model as the resonances E_A=138.7 MeV, E_B=125.4 MeV, and E_C=112.7 MeV, respectively, with a high degree of confidence based on the following grounds: (i) the theoretically predicted I=$44\hbar$ state at E_{44} = 143 MeV in Ref. [16] is close to the observed experimental resonance energy E_A=138.7 MeV,

(ii) the theoretical energy spacing between the I=44$\hbar$ an I=36$\hbar$ THSI states and between the I=36$\hbar$ and the I=28$\hbar$ THSI states are equal, and likewise the experimental spacing between resonances E_A and E_B and between resonances E_B and E_C are also approximate equal, and (iii) above the I=44$\hbar$ THSI state, there exist, theoretically, additional I=50$\hbar$ and 56$\hbar$ THSI states at higher energies, and there remains significant experimental cross section above the resonance E_A=138.7 MeV. Expressing E_I as

$$E_I = E_0 + [(E_I - E_0)/(\hbar^2/2mR^2)] \times (\hbar^2/2mR^2), \quad (3)$$

we find by using the quantity $[[(E_I - E_0)/(\hbar^2/2mR^2)]$ in Table II that E_0= 91.82 MeV and R=5.56 fm, with which we can determine E_I of all other THSI states presented in Table II. Table II reveals that up to 4p-4h excitations, the toroidal shell model predicts 10 THSI yrast states built on the toroidal I=0 core. They occur within the range of excitation energies of the present measurement. Note that some of the states are doubly degenerate.

Based upon the above THSI energy levels E_I as primary ingredients, we have constructed a simple phenomenological semi-empirical formula to estimate the relative THSI production cross sections by including the width parameters σ_I. We start by assuming that the 7α cross section obtained after subtracting the uncorrelated cross section from the correlated cross section in Fig. 2(b) arises dominantly from toroidal configurations. We assume further that the reaction cross section above the observed threshold is proportional to the distribution of deposited angular momentum I which is governed by the impact parameter and the collision dynamics.

For toroidal THSI production, the energy and angular momentum must match that of a THSI state. Hence the sum over I with (dI)=1 is carried out for THSI states. Neglecting other unknown factors, we developed the following semi-empirical cross section formula for the 7α channel from toroidal configurations

$$\sigma_{\rm toroidal}(E_x, 7\alpha) = A \sum_{I=I_{\rm toroid}} \frac{g_I I}{1+\exp\{(I-I_{\rm max})/a\}} \times \frac{1}{\sqrt{2\pi}\sigma_I} \exp\{-(E_x - E_I)^2/2\sigma_I^2\}, \quad (4)$$

where gi is the state degeneracy factor and $I_{\rm max}$ and the diffusion parameter a are introduced phenomenologically to describe initial-state dynamical and/or final-state structural limitations.

The most important primary ingredients in the above formula are the THSI spin I, energies E_I, and degeneracies g_I. Upon using the toroidal shell model of Table II to fix these primary ingredients, we extract the secondary quantities of the widths and other parameters. We find that the gross features of the excitation function can be well described by the semi-empirical formula (4) with extracted widths and fitting parameters as shown in Fig 4.

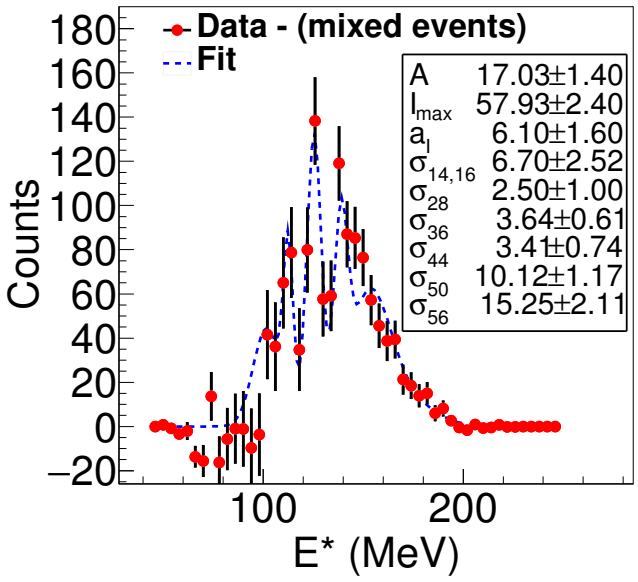

FIG. 4: The experimental (correlated data) - (mixed event data) (in solid points) are compared with the results of semi-empirical formula (4) containing the signature of the toroidal high-spin isomers as primary ingredients (in solid curve) with the list of extracted widths and other parameters.

The extracted widths for the sharp I=44$\hbar$, 36$\hbar$ and 28$\hbar$ resonances are small, of the order of the experimental bin size. The extracted widths for the I=50$\hbar$ and 56$\hbar$ states are large, which may indicate that the particle-hole excitations for these highest lying THSI states may involve promoting particles to populate states with large intrinsic widths close to the particle drip line. However, low statistical uncertainities and uncertainities in background in that region may contribute to the apparent broadening.

The present analysis indicates that the a spinning toroidal ^{28}Si* would express itself as a set of THSI states with a unique signature listed in Column 3 of Table II. In the excitation energy spectrum different facets of the toroidal signature could be found, i.e, the presence of sharp resonances at appropriate energies, the spacing between some of the resonances, the apparent presence of THSI states at energies higher than the predicted I=44$\hbar$ state.

The approximate matching of the experimental excitation energy spectrum with the semi-empirical cross section formula containing all THSI states up to 4p-4h excitations as exhibited in Fig. (4), provides support for the possible production of toroidal high-spin isomers in the present experiment.

ADDITIONAL THEORETICAL SUPPORT FROM RELATIVISTIC MEAN-FIELD CDFT THEORY

Our experimental results and the phenomenological analysis suggest the existence of more than one stabilized state. Previous non-relativistic adiabatic calculations without a toroidal shape constraint give only the I=44$\hbar$ state [16], and cannot be used to calculate diabatic THSI states such as those with I<44$\hbar$. The phenomenological description of the toroidal shell model predicts a total of 10 THSI states built on the toroidal I=0 core. These toroidal isomers states can be searched for and examined by the covariant density functional theory (CDFT) [51], which exploits basic properties of QCD at low energies, in particular, symmetries and the separation of scales. It is worth pointing out that the CDFT theory has provided an excellent description of ground states and excited (diabatic) states for nuclei all over the periodic table with a high predictive power [52–54]. Using a universal density functional and without assuming the existence of clusters *a priori*, CDFT provides a high degree of confidence in the investigation of nuclear toroidal structures.

With the most successful density functionals PC-PK1 [55] and DD-ME2 [56], the newly-developed cranking CDFT in 3D lattice space [57, 58] has been applied to investigate the toroidal states in ^{28}Si. In these calculations, the z axis is chosen as the symmetry axis. Grid points $34 \times 34 \times 24$ are respectively taken for x, y and z with a step size 0.8 fm. The self-consistency of calculations is achieved with an accuracy of 10^{-4} MeV for the single-particle levels. The pairing correlations are neglected.

By choosing a trial initial wave function with ring-like configuration of seven α-particles on the plane with $z = 0$, a toroidal state with $I = 44\hbar$ is obtained at rotational frequency $\hbar\omega = 2.5$ MeV, corresponding to 3p-3h configurations for both neutrons and protons. The excitation energy of this toroidal state is 147.93 MeV for PC-PK1 and 145.08 MeV for DD-ME2.

Local energy minima are found for the toroidal state with I=28$\hbar$, corresponding to 2p-2h excitations for both neutrons and protons, and the toroidal state with I=36$\hbar$, corresponding to the 2p-2h excitation for neutrons and 3p-3h for protons. The toroidal state with $I = 44\hbar$ can be easily obtained by the adiabatic CDFT calculations. For the toroidal states with $I = 28\hbar$ and 36$\hbar$, diabatic or configuration-fixed CDFT calculations are necessary. Additional toroidal states with I=0$\hbar$, 14$\hbar$, 16$\hbar$, 50$\hbar$ and 56$\hbar$ have also been located. They are shown in Table III and IV, respectively. In the column of $\hbar\omega$, the mid-points of a range of the cranking rotational frequencies are given for toroidal diabatic (excited) state configurations arising from particle-hole excitations without specifying $\hbar\omega$.

In order to investigate the stability of these high-spin torus isomers against particle emission, we have examined the radial density distributions of the occupied single-particle levels as well as the total density distributions for these toroidal states. As an example, neutron densities in toroidal state with $I = 28\hbar$ are shown in figure 5. It can be clearly seen that all radial density distributions are well localized and the stability of the toroidal isomer against particle emission is hereby demonstrated.

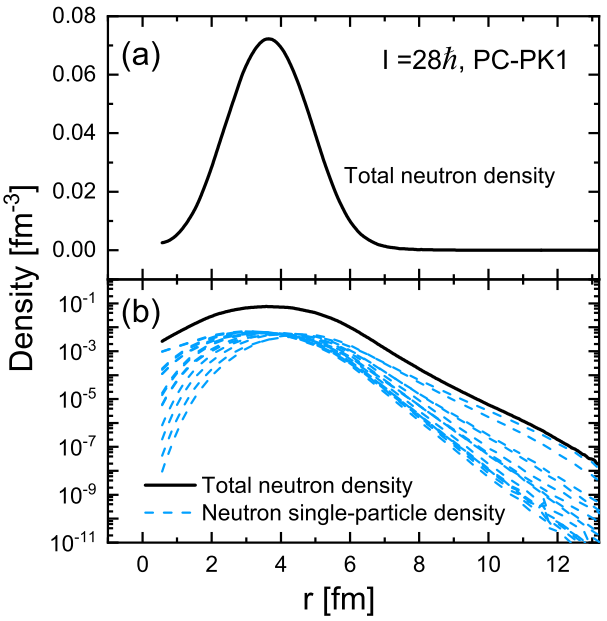

FIG. 5: Neutron radial density distributions (z direction is integrated) of the occupied single-particle levels (blue and thin lines) as well as the total density distribution (black and thick lines) in toroidal state with $I = 28\hbar$.

TABLE III: Properties of toroidal states in ^{28}Si obtained by the covariant functional PC-PK1 [55]. In the table, $\hbar\omega$ is rotational frequency, β_{20} is quadrupole deformation, related to the quadrupole moment $\langle Q_{20}\rangle$ of [16] by β_2=$\langle Q_{20}\rangle/[(3/\sqrt{5\pi})A^{5/3}r_0^2]$ with r_0=1.2 fm, E^* is excitation energy, and R, d, and $\rho_{\max}$ are determined by fitting the calculated density distributions to the Gaussian function $\rho(x,y,z) = \rho_{\max}e^{-[(\sqrt{x^2+y^2}-R)^2+z^2]/(d^2/\ln 2)}$.

I [$\hbar$]	Configuration	$\hbar\omega$ [MeV]	β_{20}	E^* [MeV]	R [fm]	d [fm]	$\rho_{\max}$ [fm^{-3}]
0	$(0p0h)_\nu(0p0h)_\pi$	—	−1.29	72.65	3.37	1.32	0.167
14	$(0p0h)_\nu(2p2h)_\pi$	—	−1.42	91.04	3.53	1.34	0.156
14*	$(2p2h)_\nu(0p0h)_\pi$	—	−1.43	91.34	3.54	1.34	0.156
16	$(1p1h)_\nu(1p1h)_\pi$	—	−1.42	89.56	3.53	1.33	0.158
28	$(2p2h)_\nu(2p2h)_\pi$	∼2.49	−1.54	106.26	3.68	1.34	0.149
36	$(2p2h)_\nu(3p3h)_\pi$	∼2.58	−1.76	128.14	3.96	1.34	0.137
36*	$(3p3h)_\nu(2p2h)_\pi$	—	−1.77	128.45	3.98	1.34	0.137
44	$(3p3h)_\nu(3p3h)_\pi$	∼2.81	−2.02	147.92	4.27	1.34	0.127
50	$(3p3h)_\nu(4p4h)_\pi$	—	−2.38	167.95	4.68	1.34	0.116
50*	$(4p4h)_\nu(3p3h)_\pi$	—	−2.39	168.18	4.69	1.34	0.115
56	$(4p4h)_\nu(4p4h)_\pi$	∼2.71	−2.79	185.18	5.11	1.34	0.106

TABLE IV: Same as Table. III but for the covariant functional DD-ME2 [56].

$I/\hbar$	Configuration	$\hbar\omega$ [MeV]	β_{20}	E^* [MeV]	R [fm]	d [fm]	$\rho_{\max}$ [fm^{-3}]
0	$(0p0h)_\nu(0p0h)_\pi$	∼0.01	−1.24	65.31	3.31	1.24	0.190
14	$(0p0h)_\nu(2p2h)_\pi$	—	−1.35	85.11	3.43	1.26	0.177
14*	$(2p2h)_\nu(0p0h)_\pi$	—	−1.36	85.53	3.45	1.26	0.177
16	$(1p1h)_\nu(1p1h)_\pi$	—	−1.35	83.42	3.44	1.25	0.179
28	$(2p2h)_\nu(2p2h)_\pi$	∼2.70	−1.46	101.08	3.58	1.27	0.168
36	$(2p2h)_\nu(3p3h)_\pi$	∼2.76	−1.68	124.32	3.85	1.28	0.151
36*	$(3p3h)_\nu(2p2h)_\pi$	—	−1.69	124.73	3.87	1.28	0.151
44	$(3p3h)_\nu(3p3h)_\pi$	∼2.88	−1.95	145.07	4.18	1.30	0.136
50	$(3p3h)_\nu(4p4h)_\pi$	—	−2.35	165.85	4.64	1.32	0.118
50*	$(4p4h)_\nu(3p3h)_\pi$	—	−2.37	166.13	4.66	1.32	0.118
56	$(4p4h)_\nu(4p4h)_\pi$	∼2.64	−2.83	183.27	5.14	1.34	0.104

Similar conclusions can be drawn for other toroidal states as well.

Results from the CDFT theory confirm the previous theoretical result predicting a toroidal high-spin isomer state with I=44$\hbar$ at an excitation energy of E_x 145 - 148 MeV, and support the identification of the resonance observed experimentally at E_x=138 MeV as this possible toroidal state. In addition all THSI states obtained in the toroidal shell model have also been located in the relativistic mean-field CDFT theory, supporting the use of the THSI states in the toroidal shell model as the signature for toroidal high-spin isomers.

There is however one notable difference that may reveal new physics associated with the toroidal shape. The spacings between energy levels in the relativistic CDFT theory appear to be significantly greater than their corresponding spacings in the toroidal shell model, or in the experimental data. One interesting possibility may be that the toroidal THSI nuclei under consideration have such a distorted shape and low densities that they may probe the nuclear energy density functional in a new regime for which the extrapolation from the normal nuclear matter in the CDFT theory may not be adequate. The possibility of using toroidal nuclei to probe the nuclear density functional at lower density may add an interesting dimension to the study of toroidal high-spin isomers.

SUMMARY AND CONCLUSIONS

In conclusion, the excitation function of the 7α channel in deep-inelastic collisions of ^{28}Si on ^{12}C reveals resonance structures at high excitation energies. The features of these structures appear to coincide with those predicted by a number of theoretical calculations in which the toroidal shell effects stabilize the nucleus in a diabatic I=0 state against major radius variations while spin-aligning particle-hole expectations lead to many high-spin toroidal isomers. If toroidal configurations are produced, the observed final distribution normally results from processes in which an initial breakup into larger excited fragments is followed by alpha particle de-excitation of those fragments. From the theoretical perspective, if the present results are confirmed by further studies, a very large number of diabatic and adiabatic toroidal high-spin isomers in a very large light-mass region may be opened up for future investigations.

Finally, we note that recent experimental and theoretical works provide indications that clustering effects are important in the collisions of α-conjugate nuclei [59, 60]. The latter work, published as this paper was being prepared for submission provides further theoretical indications that toroidal α-particle substructures may be quite commonly produced in such collisions. We strongly encourage further experimental work on collisions of light α-conjugate systems, both for the production of exotic clustered states and for the investigation of the dynamical evolution during such collisions. A higher granularity detector system and addition of gamma ray detection could offer significant improvements for such studies.

ACKNOWLEDGEMENTS

This work was supported by the United States Department of Energy under Grant # DE-FG03-93ER40773 and under grant # DE-AC05-00OR22725 with UT-Battelle, LLC (Oak Ridge National Laboratory) and by The Robert A. Welch Foundation under Grant # A0330. Partial support by the National Natural Science Foundation of China under Contracts No. 11421505, No. 11335002, No. 11621131001, and No. 11305239, the Youth Innovation Promotion Association CAS (No. 2017309) and the National Key R & D Program of China under Contract No. 2018YFA0404404 are acknowledged. Travel support for C. Y. Wong under the CUSTIPEN Program is thankfully acknowledged. We appreciate useful communications from A. Ono, J. Maruhn, T. Ichikawa and S. Umar. We also greatly appreciate the efforts of the staff of the TAMU Cyclotron Institute.

[1] N. J. Stone, Atom. Dat. Nucl. Dat. Tab. **90**, 75 (2005).
[2] S. Cohen, F. Plasil and W. J. Swiatecki, Ann. Phys. (NY) **82**, 557 (1974).
[3] J. A. Wheeler, Nucleonics Notebook, 1950 (unpublished), see also p. 297 in G. Gamow, Biography of Physics, Harper & Brothers Publishers, N.Y. 1961; Princeton University Graduate Course Physics 576 Take-Home Examination Problem 2, May 22, 1963 (unpublished).

[4] R. A. Brown and L.E. Scriven, Proc. R. Soc. Lond. A **371**, 331 (1980).
[5] S. Åberg, H. Flocard and W. Nazerewicz, Ann. Rev. Nuc. Part. Sci, **40**, 439 (1990).
[6] C. Y. Wong, Phys. Lett. **B41**, 446 (1972).
[7] C. Y. Wong, Ann. Phys. (NY) **77**, 279 (1973).
[8] C. Y. Wong, in Superheavy Elements, ed. M. A. K. Lodhi (Pergamon Press,New York, 1978) p. 524.
[9] R. Najman, R. Planeta, A. Sochocka, F. Amorini, L. Auditore, T. Cap, G. Cardella, E. DeFilippo, E. Geraci, A. Grzeszczuk, S. Kowalski, T. Kozik, G. Lanzalone, I. Lombardo, Z. Majka, N.G. Nicolis, A. Pagano, E. Piasecki, S. Pirrone, G. Politi, F. Rizzo, P. Russotto, K. Siwek-Wilczynska, I. Skwira-Chalot, A. Trifiro, M. Trimarchi, J. Wilczynski, W. Zipper, Phys. Rev. C **92**, 064614 (2015).
[10] C. Y. Wong, Phys. Rev. C **17**, 331 (1978).
[11] C. Y. Wong, Phys. Rev. Lett. **55**, 1973 (1985).
[12] J. Y. Zhang and C. Y. Wong, Phys. Rev. C **34**, 1094 (1986).
[13] W. Zhang, H. Z. Liang, S. Q. Zhang, J. Meng, Chin. Phys. Lett. **27**, 102103 (2010).
[14] T. Ichikawa, J. A. Maruhn, N. Itagaki, K. Matsuyanagi, P. G. Reinhard, S. Ohkubo, Phys. Rev. Lett. **109**, 232503 (2012).
[15] T. Ichikawa, K. Matsuyanagi, J. A. Maruhn, N. Itagaki, Phys. Rev. C **89**, 011305(R) (2014); ibid., **90**, 034314 (2014).
[16] A. Staszczak and C. Y. Wong, Phys. Lett. **B738**, 401 (2014).
[17] A. Staszczak and C. Y. Wong, Acta Phys. Pol. B **46**, 675 (2015).
[18] A. Staszczak and C. Y. Wong, Phys. Scr. **90**, 114006 (2015).
[19] M. Brack, J. Damgaard, A. S. Jensen, H.C. Pauli, V. M. Strutinsky, C. Y. Wong, Rev. Mod. Phys. **44** 320 (1972).
[20] A. Bohr and B. Mottelson, Nucl. Phys. **A345**, 303c (1981).
[21] M. Ploszajczak *et al.*, Nucl. Phys. **A301**, 477(1978).
[22] M. B. Tsang *et al.*, Eur. Phys. J. A **30**, 129 (2006).
[23] J. Plateau, Annual Report of the Board of Regents of the Smithsonian Institution, **207**, (1863); ibid., **286** (1865); ibid., **255** (1866).
[24] Lord Rayleigh, Phil. Mag. **28**, 161 (1914).
[25] E. Pairam and A. Fernández-Nieves, Phys. Rev. Lett. **102**, 234501 (2009).
[26] A. K. Nurse, S. R. Coriell and G. B. McFadden, J. Res. NIST **120**, 74 (2015).
[27] M. A. Fontelos, V. J. Garcia-Garrido, and U. Kindelán, SIAM J. Appl. Math. **71** (6), 1941 (2011).
[28] H. Hofmann, "The Physics of Warm Nuclei: With Analogies to Mesoscopic Systems", Oxford University Press, USA (2008).
[29] Clusters in Nuclei, ed. C. Beck, Springer International Publishing, **1** (2010); ibid., **2** (2012); ibid., **3** (2014).
[30] K. Ikeda, N. Tagikawa and H. Horiuchi, Prog. Theor. Phys. Suppl. E **68**, 464 (1968).
[31] W. von Oertzen, M. Freer and Y. Kanada-En'yo, Phys. Rep. **432**, 43 (2006).
[32] M. Freer, Rep. on Prog. in Phys. **70** 2149.(2007).
[33] Y. Kanada-En'yo, H. Horiuchi, Prog. Theor. Phys. Suppl. **142**, 205 (2001).
[34] Y. Funaki, T. Yamada, H. Horiuchi, G. Röpke, P. Schuck, and A. Tohsaki, Phys. Rev. Lett. **101** 082502 (2008).
[35] D. H. Wilkinson, Nucl. Phys. **A452**, 296 (1986).
[36] W. von Oertzen and M. Milin , Covalent Binding on the Femtometer Scale: Nuclear Molecules, Clusters in Nuclei - Vol.3 - Lecture Notes in Physics Springer Heidelberg, **875**, 147 (2014).
[37] K. Hagel, M. Gonin, R. Wada, J. B. Natowitz, F. Haddad, Y. Lou, M. Gui, D. Utley, B. Xiao, J. Li, G. Nebbia, D. Fabris, G. Prete, J. Ruiz, D. Drain, B. Chambon, B. Cheynis, D. Guinet, X. C. Hu, A. Demeyer, C. Pastor, A. Giorni, A. Lleres, P. Stassi, J. B. Viano, P. Gonthier, Phys. Rev. C **50**, 2017 (1994).
[38] Y. Larochelle, L. Beaulieu, G. Anctil, B. Djerroud, D. Dore, R. Laforest, J. Pouliot, R. Roy, M. Samri, C. St-Pierre, G. C. Ball, D. R. Bowman, A. Galindo-Uribarri, E. Hagberg, D. Horn, D. Guinet, P. Lautesse, Phys. Rev. C **53**, 823 (1996).
[39] A. Ono, Phys. Rev. C **59**, 853 (1999).
[40] W. Cassing, Z. Phys. **A327**, 87 (1987).
[41] R. J. Charity, Phys. Rev. C **82**, 014610 (2010).
[42] D. Mancusi, R. J. Charity and J. Cugnon, Phys. Rev. C **82**, 044610 (2010).
[43] D. Lacroix, A. Van Lauwe, and D. Durand, Phys. Rev. C **69**, 054604 (2004).
[44] W. W. Wilcke *et al.*, Atom. Dat. Nucl. Dat. Tab. **25**, 389 (1980).
[45] S. Wuenschel *et al.*, Nucl. Instr. Meth. Phys. Res. **A604**, 578 (2009).
[46] R. Wada, T. Keutgen, K. Hagel, Y. G. Ma, J. Wang, M. Murray, L. Qin, P. Smith, J. B. Natowitz, R. Alfarro, J. Cibor, M. Cinausero, Y. El Masri, D. Fabris, E. Fioretto, A. Keksis, S. Kowalski, M. Lunardon, A. Makeev, N. Marie, E. Martin, Z. Majka, A. Martinez-Davalos, A. Menchaca-Rocha, G. Nebbia, G. Prete, V. Rizzi, A. Ruangma, D. V. Shetty, G. Souliotis,P. Staszel, M. Veselsky, G. Viesti, E. M. Winchester, S. J. Yennello, W. Zipper, A. Ano, Phys. Rev. C **69**, 044610(2004).
[47] W. Lin, X. Liu, M. R. D. Rodrigues, S. Kowalski, R. Wada, M. Huang, S. Zhang, Z. Chen, J. Wang, Gl Q. Xiao, R. Han, Z. Jin, J. Liu, P. Ren, F. Shi, T. Keutgen, K. Hagel, M. Barbui, C. Bottosso, A. Bonasera, J. B. Natowitz, T. Materna, L. Qin, P. K. Sahu, H. Zheng, Phys Rev C **90**, 044603 (2014).
[48] S. I. Bityukov and N. V. Krasnikov, arXiv:physics 9809037v2 (1998).
[49] G. Fai and J. Randrup, Nucl. Phys. **A404**, 551 (1983).
[50] J. P. Bondorf, C. H. Dasso, R. Donangelo and G. Pollarolo, Phys. Lett. **B240**, 28 (1990).
[51] J. Meng, ed., Relativistic Density Functional for Nuclear Structure, International Review of Nuclear Physics, Vol. 10 (World Scientfic, Singapore, 2016).
[52] J. Meng, J. Peng, S. Q. Zhang, P. W. Zhao, Front. Phys. **8**, 55 (2013).
[53] J. Meng, H. Toki, S.-G. Zhou, S. Zhang, W. Long, and L. Geng, Progress in Particle and Nuclear Physics **57**, 470 (2006).
[54] H. Z. Liang, J. Meng, and S.-G. Zhou, Physics Reports **570**, 1 (2015).
[55] P. W. Zhao, Z. P. Li, J. M. Yao and J. Meng, Phys. Rev. C **82**, 054319 (2010).
[56] G. A. Lalazissis, T. Nikšić and D. Vretenar, P. Ring, Phys. Rev. C **71**, 024312 (2005).
[57] Z. X. Ren, S. Q. Zhang, J. Meng, Phys. Rev. C **95**, 024313 (2017).
[58] Z. X. Ren *et al.*, to be published.

[59] K. Schmidt, X. Cao, E. J. Kim, K. Hagel, M. Barbui, J. Gauthier, S. Wuenschel, G. Giuliani, M. R. D. Rodrigues, H. Zheng, M. Huang, N. Blando, A. Bonasera, R. Wada, C. Botosso, G. Liu, G. Viesti, S. Moretto, G. Prete, S. Pesente, D. Fabris, Y. El Masri, T. Keutgen, S. Kowalski, A. Kumar, G. Zhang, J. B. Natowitz, Phys. Rev. C **95**, 054618 (2017).

[60] B. Schuetrumpf and W. Nazarewicz, Phys. Rev. C **96**, 064608 (2017).